Top Catal (2014) 57:526–537
DOI 10.1007/s11244-013-0209-9

ORIGINAL PAPER

Effect of Structural Promoters on Fe-Based Fischer–Tropsch Synthesis of Biomass Derived Syngas

Pratibha Sharma · Thomas Elder · Leslie H. Groom · James J. Spivey

Published online: 26 November 2013

Abstract Biomass gasification and subsequent conversion of this syngas to liquid hydrocarbons using Fischer–Tropsch (F–T) synthesis is a promising source of hydrocarbon fuels. However, biomass-derived syngas is different from syngas obtained from other sources such as steam reforming of methane. Specifically the H_2/CO ratio is less than 1/1 and the CO_2 concentrations are somewhat higher. Here, we report the use of Fe-based F–T catalysts for the conversion of syngas produced by the air-blown, atmospheric pressure gasification of southern pine wood chips. The syngas from the gasification step is compressed and cleaned in a series of sorbents to produce the following feed to the F–T step: 2.78 % CH_4, 11 % CO_2, 15.4 % H_2, 21.3 % CO, and balance N_2. The relatively high level of CO_2 suggests the need to use catalysts that are active for CO_2 hydrogenation as well is resistant to oxidation in presence of high levels of CO_2. The work reported here focuses on the effect of these different structural promoters on iron-based F–T catalysts with the general formulas 100Fe/5Cu/4K/15Si, 100Fe/5Cu/4K/15Al and 100Fe/5Cu/4K/15Zn. Although the effect of Si, Al or Zn on iron-based F–T catalysts has been examined previously for CO+CO_2 hydrogenation, we have found no direct comparison of these three structural promoters, nor any studies of these promoters for a syngas produced from biomass. Results show that catalysts promoted with Zn and Al have a higher extent of reduction and carburization in CO and higher amount of carbides and CO adsorption as compared to Fe/Cu/K/Si. This resulted in higher activity and selectivity to C_5+ hydrocarbons than the catalyst promoted with silica.

Keywords Biomass syngas · Fischer–Tropsch synthesis · Fe based catalysts · Structural promoters

P. Sharma · J. J. Spivey (✉)
Department of Chemical Engineering, Louisiana State University, S.Stadium Drive, Baton Rouge, LA 70803, USA
e-mail: jjspivey@lsu.edu

T. Elder · L. H. Groom
USDA Forest Service, Southern Research Station, Pineville, LA 71360, USA

1 Introduction

Due to increasing oil prices, depletion of fossil fuel reserves and increased environmental concerns, biomass has received attention as a source of clean energy [1]. Fuels derived from biomass have very low sulphur content, generally excellent fuel properties [2, 3] with low lifecycle CO_2 emissions [4]. One process for converting biomass to clean fuels is through gasification and subsequent Fischer–Tropsch Synthesis (FTS).

The Fischer–Tropsch reaction is usually studied using a synthetic mixture of CO and H_2 [5, 6], with far fewer studies using CO_2 and hydrogen [7, 8]. Even fewer studies have examined FTS using a mixture of CO, H_2, and the high levels of CO_2 present in biomass-derived syngas [9, 10]. The high concentrations of CO_2 in biomass-derived syngas have two important effects. First, CO_2 can affect the hydrogenation reactions in FTS since the reverse water gas shift competes with CO hydrogenation [11]. Second, the iron-based catalysts used in FTS may be subject to deactivation by oxidation of the active iron carbide phase in the presence of high concentrations of CO_2 [8, 9].

Biomass-derived syngas also typically contains lower concentrations of hydrogen than needed to produce hydrocarbon fuels, e.g. H_2/CO ratio is less than 1/1 [12, 13]. Of the studies on CO + CO_2 hydrogenation with iron-based

catalysts [8, 9, 11, 14], there are very few studies in which the H_2/CO ratio is less than 1/1. Yates and Satterfield [15] studied CO+CO_2 hydrogenation of a hydrogen deficient syngas (H_2/CO $\sim$0.67–0.71) on fused magnetite catalysts. They reported that CO_2 was relatively inert at fixed partial pressures of CO+H_2. Chun et al. [16] studied the hydrogenation of CO_2-rich syngas with a H_2/CO ratio of $\sim$1 on Fe/Cu/K/Si catalyst and found that CO_2 in the feed stream lowered both the rate of hydrocarbon formation as well CO_2 formation from WGS. These differing conclusions are generally believed to be due to different reaction conditions and catalysts formulations [16].

In the present study, we carry out FTS of a syngas which has high levels of CO_2 and is obtained by the air-blown, atmospheric pressure gasification of wood chips. The composition of this syngas after dehydration and contaminant removal at the gasifer site is 2.78 % methane, 11 % CO_2, 15.4 % H_2, 21.3 % CO and balance N_2. The high concentration of N_2 lowers the partial pressures of the reactants, greatly decreasing the overall rate, and may affect the selectivity as well.

There are very few studies that have examined the effect of structural promoters on hydrogenation of CO_2, and even fewer on the hydrogenation of CO+CO_2 mixtures. Jun et al. [9] compared co-precipitated Fe/Cu/K/Al and Fe/Cu/K/Si using a synthetic syngas containing 11 % CO, 32 % CO_2, 5 % Ar and 52 % H_2. They found that stability of the iron carbide phases in Fe/Cu/K/Al was higher than that of Fe/Cu/K/Si, resulting in the higher activity of the catalyst in the presence of high levels of CO_2.

Three iron-based catalysts are reported here: 100Fe/5Cu/4 K/15x where x is Si, Al or Zn which are added as structural promoters. These promoters have been previously studied individually for CO_2 hydrogenation as well as hydrogenation of CO+CO_2 mixtures [9, 11], but have not been directly compared. The objective of studying these specific catalysts is to directly compare the extent of carburization and resistance to oxidation in presence of CO_2 while actively hydrogenating CO and CO_2 to hydrocarbons.

2 Experimental

2.1 Catalyst Preparation

The catalysts were prepared by the technique of co-precipitation [17]. Base catalyst of 100Fe/5Cu/15x was prepared by co-precipitating the aqueous solutions of the salts at constant pH, where x is Si, Al or Zn. In the process, 1.4 M solution of Fe$(NO_3)_3{\cdot}9H_2O$ (Aldrich 99.99 %), and 3 M solution of $Cu(NO_3)_2{\cdot}3H_2O$ (Aldrich 99.99 %) were first mixed together in deionized water. In a separate beaker $Al(NO_3)_3{\cdot}9H_2O$ (Aldrich 99.9 %), $Zn(NO_3)_2{\cdot}6H_2O$ (Aldrich 99.99 %) or tetraethylorthosilicate ($Si(OC_2H_5)_4$, Aldrich 99 %) were dissolved in 40 ml of ethanol and stirred continuously. The solutions were then mixed together to a volume of 100 ml and heated to a temperature of 80 $\pm$ 3 °C. Alongside, 1 M solution of ammonium carbonate ($(NH_4)_2CO_3$, Aldrich 99.999 %) was also heated to a temperature of 80 $\pm$ 3 °C and the solutions were co-precipitated under vigorous mixing at a constant pH of 7–7.5. After co-precipitation, the solution was allowed to age for 18 h and the precipitate was filtered and washed to remove all soluble ions. After washing and filtering, the precipitate was dried in an oven at 120 °C for 24 h. The dried precipitate was crushed and sieved through 120 mesh and catalyst powder of particle size less than 125 microns was obtained.

The catalysts were further impregnated with potassium bicarbonate ($KHCO_3$) using incipient wetness impregnation method to obtain the final composition of 100Fe/5Cu/4 K/15x.

The impregnated catalysts were calcined in a muffle furnace with a ramp at a rate of 5°/min to the calcination temperature of 350 °C, which was held for 5 h in flowing air at a flow rate of 100 ml/min. The furnace was cooled to room temperature at a rate of 5 °C/min [18]. The catalysts were finally designated as Fe/Cu/K/Si, Fe/Cu/K/Al and Fe/Cu/K/Zn.

3 Catalyst Characterization

3.1 X-Ray Diffraction

For studying the crystalline nature of the freshly calcined catalysts using X-Ray diffraction, experiments were done on a Bruker/Siemens D5000 X-ray diffraction set up. The instrumentation consisted of a ceramic X-ray tube with Cu Kα radiation of 1.54184 Å. The voltage for the X-Ray tube was 40 kV and the current was 30 mA. The setting of the anti-scatter slit was adjusted at 0.5°, while the angle of divergence slit for incident X-Ray beam was set at 1°. For analysis, the scan was done from 20 ° to 90 ° with a step size of 0.05°/min.

3.2 BET Surface Area Measurement

Brunauer–Emmett–Teller (BET) surface area of the freshly calcined catalysts was determined using N_2 physisorption at 77 K in AMI 200HP (Altamira instruments). Before physisorption, 0.05 g of the sample was first heated in Helium (He) to a temperature of 150 °C, to remove any moisture if present.

3.3 Inductively Coupled Plasma–Optical Emission Spectroscopy (ICP–OES)

The bulk elemental composition of the fresh catalysts was determined using the technique of ICP–OES on a Perkin

Elmer 2000 DV instrument. The samples were first weighed to nearest 0.00001 g in a Teflon bottle, and 5 mL of aqua regia was added to each sample. The sample was allowed to sit overnight. 5 ml of HF was added to each sample and the samples were heated to ~95 °C until they completely dissolved in HF. The volume was brought to 100 ml by adding deionized water. A blank analysis was also performed in the similar manner.

3.4 Scanning Electron Microscopy (SEM) and Energy Dispersive X-ray (EDX) Analysis

Scanning electron microscopy (SEM) and Energy dispersive X-Ray (EDX) was done on freshly calcined catalysts to study the morphology and the elemental distribution of the external catalyst surface. The instrumentation for SEM and EDX was a JEOL JSM-5910-LV SEM with an EDAX UTW-Phoenix detector using Genesis software. The catalyst was uncoated and set up to run the elements selected for each group using the EDS spectrums for each material.

3.5 H_2 Temperature Programmed Reduction (H_2 TPR)

Temperature programmed reduction of catalysts in H_2 was done on Altamira (AMI 200 HP) instrument. 0.03 g of a sample was placed in a quartz cell (6.5 inch (length) by 6 mm (outer diameter) by 4 mm (inner diameter)) and packed with quartz wool. The bed temperature was measured continuously by a thermocouple which ran axially through the tube touching the quartz wool. The catalyst was first oxidized completely by treating it with 10 % O_2/He flowing at 50 ml/min with temperature ramp from room temperature to 400 °C at 5 °C/min and held for 30 min. The gas flow was switched to He and the catalyst was cooled to room temperature. 10 % H_2/Ar was then allowed to flow at a rate of 30 ml/min, and the temperature was ramped at 5 °C/min to 950 °C. The signal was measured in a thermal conductivity detector (TCD). For calculating the amount of H_2 consumed, silver oxide (Ag_2O), amounts 0.1 g and 0.15 g were also reduced in H_2 similarly, and area calibration was done to calculate amount of H_2 consumed by the iron catalysts.

3.6 CO Temperature Programmed Reduction (CO TPR)

CO TPR was done to study the reduction and carburization of the catalysts in CO. 0.03 g of the catalyst sample was placed in the quartz tube of the AMI 200 HP. For this, the catalyst sample was completely oxidized under 10 % O_2/He at 400 °C and then cooled to ambient temperature in flowing He. After oxidation, the gas was switched to 5 % CO/He at a flow of 50 ml/min and the temperature was increased to 950 °C at a ramping rate of 5 °C/min. The gas leaving the reactor was connected to a quadrupole AMETEC Mass Spectrometer (MS) instrument, and the signal for CO and CO_2 was measured.

3.7 Temperature Programmed Hydrogenation (TPH)

100 mg of the catalyst was purged with helium to a temperature of 150 °C and then subsequently cooled to ambient temperature. The catalyst was pretreated in 5 % CO/He flowing at 50 ml/min, by increasing the temperature from ambient to 280 °C at 5 °C/min, after which the temperature was held constant at 280 °C, for 24 h. After pretreatment, the catalyst was cooled to 35 °C in flowing He. Subsequently the gas was switched to 50 ml/min of 10 % H_2/Ar and the temperature was increased to 950 °C at a ramping rate of 5 °C/min. CH_4 signal was monitored in the Mass spectrometer (mass 15 was monitored instead of 16) to analyze the evolution of different carbon forms with temperature.

3.8 CO Temperature Programmed Desorption (CO TPD)

For CO TPD, 100 mg of the sample was loaded in the quartz tube and the catalyst sample was treated with flowing He with the temperature increased to 150 °C, and held for 30 min to ensure moisture removal. The sample was cooled to ambient temperature. The gas flow was then switched to 5 % CO/He, at a flow rate of 30 cc/min and the temperature was raised to 280 °C at 5 °C/min. The catalyst was held at this temperature for 6 h. After reduction and carburization, the gas flow was changed to He at 280 °C and allowed to flow over the catalyst bed for 30 min, to ensure complete removal of any adsorbed species from the catalyst surface. The temperature was then reduced to 35 °C in flowing He.

5 % CO/He at a flow rate of 50 ml/min was allowed to flow over the catalyst for 30 min at 35 °C. Helium was then passed over the catalyst until the CO baseline leveled off. TPD was done by flowing He at 30 ml/min over the catalyst, and the temperature was raised to 950 °C at a rate of 5 °C/min. The gas from the reactor was connected to the quadrupole Mass Spectrometer through a capillary tube and the signal for CO and CO_2 was measured.

3.9 Catalytic Performance Test

Catalytic activity was evaluated with a PID MA10000 Microactivity Reactor. The system has the capability to condense and store higher hydrocarbons and aqueous products as liquids in separate traps while the unconverted syngas along with lighter hydrocarbons (C_6 and less), and CO_2 exits the reactor at atmospheric pressure to be analyzed in a gas chromatograph.

The biomass derived syngas under study was obtained using the gasification process explained elsewhere [19]. The biomass derived syngas with a composition of 2.78 % CH_4, 11 % CO_2, 15.4 % H_2, 21.3 % CO, and balance N_2 was passed through a series of adsorbents and filters to remove impurities such as NH_3, HCl, H_2S, moisture etc. to less than 10 ppm prior to FTS.

Catalyst Pretreatment: 1 gm catalyst was diluted with five parts sand to avoid temperature gradients in the catalyst bed due to the exothermicity of the reaction. The temperature was increased to 280 °C in flowing helium. After reaching 280 °C, the gas flow was changed to 50 % CO/50 % He at a total flow rate of 60 ml/min. The catalyst was reduced and carburized in 50 % CO for 24 h at a pressure of 1 bar.

Reaction: After activation, the reactor was flushed with helium at 50 ml/min for 1 h. The gasflow was then switched to flow the syngas at a total GHSV of 1,800 scc $h^{-1}gcat^{-1}$, temperature of 300 °C, and the pressure of 2.8 MPa [20].

The run was allowed to continue for 144 h. The instrument has a peltier cell, which condenses the gases leaving the reactor. The peltier cell separating the liquid phase from the gases was maintained at temperature of 5 °C. The liquids were collected in a trap, while the uncondensed gases at atmospheric pressure were collected and analyzed in a Shimadzu GC-2014 gas chromatograph. The GC system consists of a FID (Flame ionization detector) used for analyzing hydrocarbons after being separated in a Restek Rt-Q-BOND column (23 m × 0.53 mm × 20 μm). The wax trap was maintained at a temperature of 145 °C for collection of wax produced during the reaction.

The aqueous phase is analyzed in a Hewlett–Packard 5790Agilent gas chromatograph (GC) with a Porapak Q packed column using a thermal conductivity detector. The oil phase is analyzed using a 6890A GC with a DB-5 capillary column and a flame ionization detector (FID). The wax phase is analyzed using 6890 Agilent GC FID with a high temperature DB-1 capillary column.

4 Results and Discussion

4.1 Catalyst Characterization

4.1.1 X-Ray Diffraction

The XRD spectra for the three freshly calcined catalysts samples shown in Fig. 1 shows that all catalysts are XRD amorphous [21], with any crystallite size being smaller than 4–5 nm based on the wavelength of the Cu Kα radiation [18]. This shows that the catalyst preparation method produced small, dispersed forms of iron.

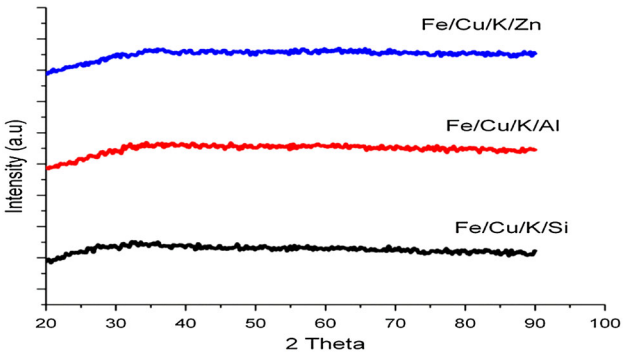

Fig. 1 X-Ray diffraction spectra for the freshly calcined catalyst samples

Table 1 BET surface area of the three catalysts

Catalyst	BET surface area (m^2/g)
Fe/Cu/K/Si	428
Fe/Cu/K/Al	360
Fe/Cu/K/Zn	276

Similarly, the XRD spectra of the passivated post run catalysts (not shown) showed no peaks, suggesting that the catalysts are XRD amorphous after reaction as well.

4.2 BET Surface Area

Table 1 shows that the BET surface area of the three catalysts after calcination are slightly higher than normal are obtained for all three catalysts, but are similar to those prepared by Lohitharn et al. [21]. using the same preparation method. The catalyst containing Si has the highest surface area (428 m^2/g), which is in agreement with previous studies showing Si containing iron catalysts to have higher surface areas than iron catalysts with Al [22, 23]. The high BET surface area also suggests the presence of smaller crystallites, in agreement with the XRD results in Fig. 1.

4.3 Bulk Composition Analysis using ICP–OES

Table 2 shows that the bulk compositions of the catalysts as determined by ICP–OES correspond to the target compositions of the atomic ratio of Fe/Me where Me is the promoter.

4.4 SEM and EDX

SEM results in Fig. 2 show that the catalyst particle size vary from 10 to 125 μ. The catalyst particles are irregularly shaped for all catalysts, and different structural promoters did not change the catalyst morphology [21], which show

Table 2 Bulk composition analysis of the catalysts using ICP–OES

Sample name	Fe wt%	Cu wt%	K wt%	Si wt%	Al wt%	Zn wt%
Fe/Cu/K/Si	54.7	2.93	1.56	4.24	–	–
Fe/Cu/K/Al	55.6	2.99	1.51	–	4.26	–
Fe/Cu/K/Zn	58.6	3.14	1.60	–	–	9.99[a]

Max error: ±5 %

[a] This wt% Zn corresponds to comparable atom % for Si and Al

uneven and faceted surfaces [18]. Since the catalysts are XRD amorphous, the SEM figures suggest that the catalyst particles must be composed of many small iron oxide crystallites bound together but prevented from sintering together due to the presence of the structural promoters [18, 21]. It has been reported that Si prevents sintering of the catalyst [24], and acts as a binding agent [25], resulting in higher surface areas than catalysts prepared from precipitation of Fe without any Si [26]. The SEM and BET surface area for the Fe/Cu/K/Al and Fe/Cu/K/Zn suggest that Al and Zn, like Si, act as binding agents for the catalyst particles, preventing the catalysts from sintering.

EDX profiles of the three catalysts shown in Fig. 3 are point averaged and show that the all metals are present on the surface of the catalysts. The Fe/Me atomic ratios on the surface of the catalysts (Me = Si, Al or Zn) are similar for the three catalysts: Fe/Si ~7.7, Fe/Al ~7.8 and Fe/Zn ~7.42, which are within the experimental error. These ratios are slightly higher than in the bulk. EDX maps (not shown) showed that all elements are evenly distributed for all the catalysts. Although Si, Zn and Al are present in higher concentrations, they do not interfere with the distribution of the other metals [18].

4.5 Temperature Programmed Reduction (TPR)

H_2 TPR of the three catalysts is shown in Fig. 4. For the reduction of pure Fe_2O_3, two main peaks are observed at 330 and 530 °C. The first peak corresponds to the reduction of Fe_2O_3 to Fe_3O_4, while the second peak is assigned to the reduction of Fe_3O_4 to Fe [27]. The two step reduction of Fe_2O_3 to Fe is as follows [27, 28].

$$3Fe_2O_3 + H_2 \rightarrow 2Fe_3O_4 + H_2O \quad (1)$$

$$Fe_3O_4 + 4H_2 \rightarrow 3Fe + 4H_2O \quad (2)$$

Cu promotes the reduction of Fe_2O_3 to Fe_3O_4 at lower temperatures than reduction of bulk Fe_2O_3 without any Cu [29, 30]. Cu crystallites nucleate during reduction and dissociatively adsorb H_2, which reduces Fe_2O_3 at lower temperatures than catalysts without Cu [31, 32]. The TPR results clearly show that pure Fe_2O_3 reduces to Fe_3O_4 at 330 °C, while in the presence of Cu; the catalysts reduce at a much lower temperature in the range of 205–244 °C, consistent with well documented results on similar catalysts [24, 29].

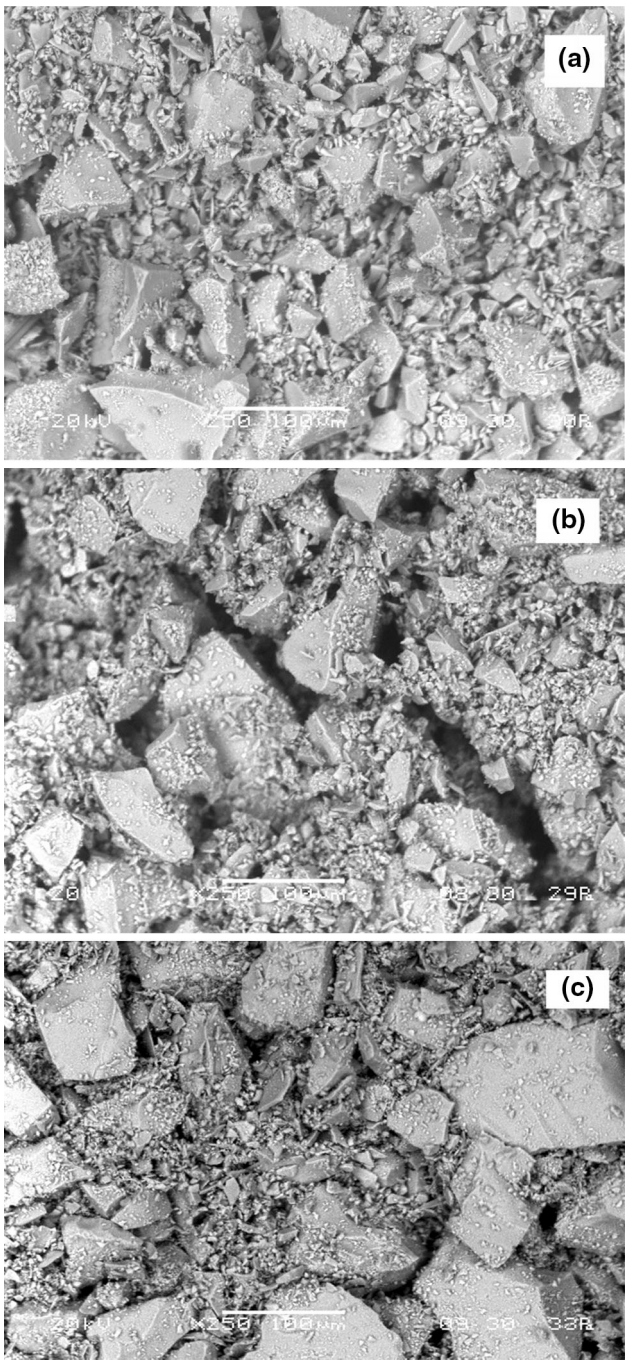

Fig. 2 SEM images of the catalysts samples- (**a**) Fe/Cu/K/Si, (**b**) Fe/Cu/K/Al, (**c**) Fe/Cu/K/Zn

For the Fe/Cu/K/Si, the first reduction peak at ~244 °C is higher than that for Fe/Cu/K/Al (~220 °C) and Fe/Cu/K/Zn (~205 °C). This may be attributed to closer interaction of Cu with Fe_2O_3 in case of Fe/Cu/K/Al and Fe/Cu/K/Zn catalysts. Previous studies have suggested that

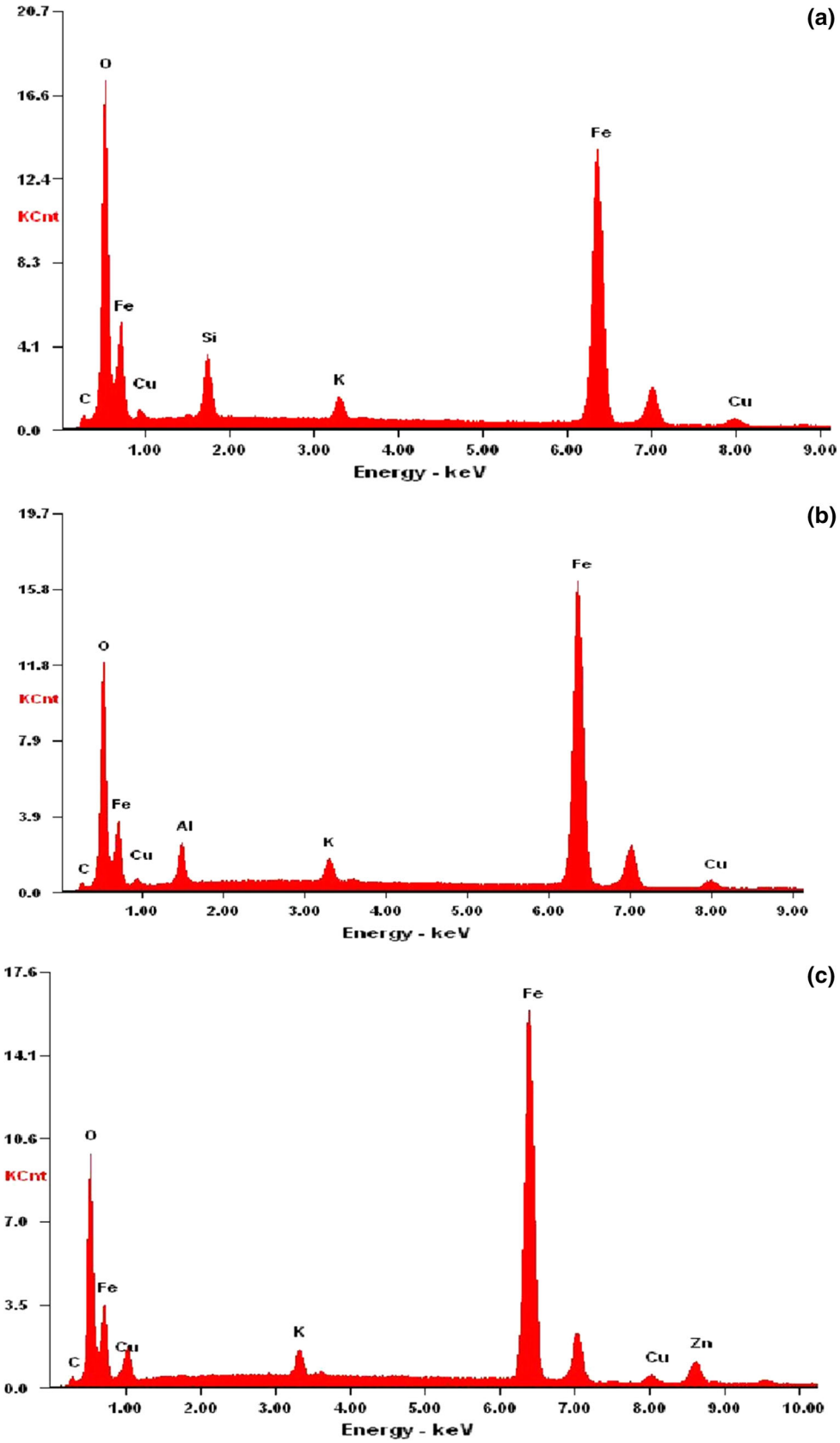

Fig. 3 EDX profiles of the catalysts samples- (**a**) Fe/Cu/K/Si, (**b**) Fe/Cu/K/Al, (**c**) Fe/Cu/K/Zn

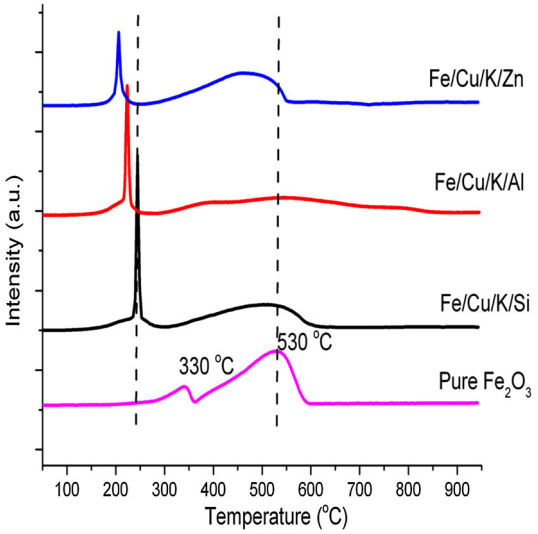

Fig. 4 Temperature Programmed reduction of the catalysts in 10 % H_2/Ar

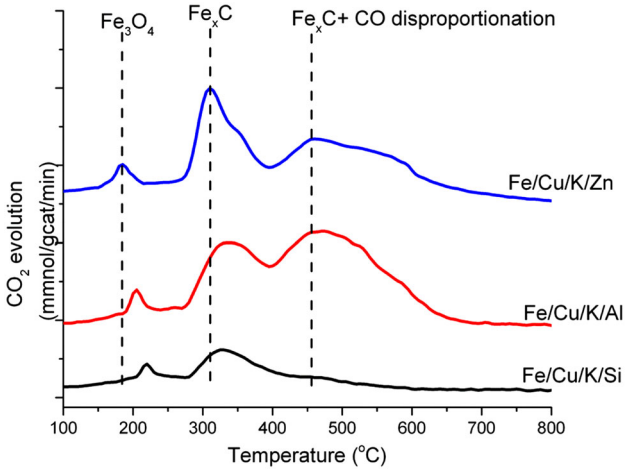

Fig. 5 CO_2 formation rate during CO Temperature Programmed Reduction of the catalysts in 5 % CO/He

incorporation of SiO_2 and Al_2O_3 retards the reduction of iron oxide due to strong metal-support interactions [28] which could be responsible for the slightly higher reduction temperature of Fe_2O_3 to Fe_3O_4 in case of Fe/Cu/K/Al and Fe/Cu/K/Si.

On Fe/Cu/K/Zn, the second reduction step, i.e. Fe_3O_4 to Fe^o (Eq. (2)), takes place at a slightly lower temperature than for Fe/Cu/K/Si. This could be either due to closer interaction with Cu or less intimate interaction of Fe with Zn as structural promoter. For Fe/Cu/K/Al, the second reduction peak is quite broad and is at a temperature comparable to that for Fe/Cu/K/Si. The reduction of Fe in presence of Al at this slightly higher temperature may be attributed to a strong interaction of Fe and Al_2O_3 [33], shifting the reduction of Fe_3O_4 to Fe to higher temperatures.

4.6 CO Temperature Programmed Reduction

CO TPR results are shown in Fig. 5. During CO temperature reduction, the oxygen removal from the lattice is followed by bulk carbide formation [34]. This occurs in two steps both of which produce CO_2 [35]:

$$3Fe_2O_3 + CO \rightarrow 2Fe_3O_4 + CO_2 \quad (3)$$

$$Fe_xO + 2CO \rightarrow Fe_xC + 2CO_2 \quad (4)$$

In Eq. (4), oxygen removal and carbide formation occur in the same step [36].

Also, during reduction CO_2 could be formed by the Bouduard reaction:

$$2CO \rightarrow C + CO_2 \quad (5)$$

The CO TPR of all three catalysts shows three peaks. Fe_2O_3 is reduced to Fe_3O_4 in the temperature range of 150–250 °C. From 260 to 405 °C, Fe_3O_4 is reduced and carburized to iron carbides (χ-carbides) [34]. Above 405 °C, transformation of the various iron carbides to stable carbide phases like cementite (Fe_3C) takes place [32]. Also above 405 °C, CO_2 formation also occurs via the Bouduard reaction [34], causing amorphous carbon to form on the catalyst.

For Fe/Cu/K/Zn the first peak for the reduction of Fe_2O_3 to Fe_3O_4 is at 185 °C, while this first peak shifts to higher temperature with Al (~205 °C) and Si (~220 °C) promotion. Also, the concurrent reduction and carburization of Fe_3O_4 for Fe/Cu/K/Zn takes place at a slightly lower temperature than Fe/Cu/K/Al or Fe/Cu/K/Si. This second peak temperature is 310 °C for Zn promoted catalyst while the peak shifts to ~330 °C for both Si and Al promoted catalysts. The TPR peak area is highest for Fe/Cu/K/Zn, indicating that more CO is consumed during this reduction and carburization than for Fe/Cu/K/Al and even less for Fe/Cu/K/Si. This suggests that the catalyst promoted with Si is the least carburized. The third peak, corresponding to both the inter-transition of iron carbides to more thermally stable iron carbides, and to CO_2 formation due to the Bouduard reaction, is also minimum in case of Si, at least as judged by CO TPR.

Table 3 shows the total amount of CO_2 evolved during the CO reduction of the catalysts, as well as CO_2 evolved during different reduction stages. This suggests that reduction in CO increases in the order of Fe/Cu/K/Zn > Fe/Cu/K/Al > Fe/Cu/K/Si.

4.7 Temperature Programmed Hydrogenation (TPH)

The iron catalysts change during pretreatment and during the reaction [37], including phase transformations during activation, with Fe_2O_3 converted to Fe_3O_4, which is then transformed to iron carbides [38–40]. It is generally

Table 3 CO_2 evolved during CO Temperature Programmed Reduction of the catalysts

Catalyst name	CO_2 evolved during Fe_2O_3 reduction to Fe_3O_4 (mmol/gcat)	CO_2 evolved during Fe_3O_4 reduction to Fe_xC (mmol/gcat)	CO_2 evolved due Bouduard reaction (mmol/gcat)	Total amount of CO_2 evolved (mmol/gcat)
Fe/Cu/K/Si	0.0012	0.0037	0.0011	0.006
Fe/Cu/K/Al	0.00155	0.0065	0.00495	0.013
Fe/Cu/K/Zn	0.00168	0.0072	0.00562	0.0145

believed that these carbides are the active phase for iron catalysts [41, 42]. The carbide phases consist of carbon atoms in octahedral interstices (ε-Fe_2C, $\acute{\varepsilon}$-$Fe_{2.2}C$ and Fe_xC), and carbides with carbon atoms in trigonal prismatic interstices (χ-$Fe_{2.5}$ C and θ-Fe_3C) [43] [37]. Bartholomew et al. used TPH of carbided catalysts to study the different metal carbides and carbon species formed during pretreatment or during FTS reaction for both supported and unsupported catalysts [44]. A series of TPH experiments were carried out on each of the catalysts of interest here (Fig. 6).

Figure 6 shows the Gaussian deconvolution of the overlapping TPH peaks to identify the various forms of carbon according to the assignments in Table 4 [40, 44]. Specifically, the peaks have been designated as α (adsorbed, atomic carbon, surface carbide), β (polymeric, amorphous aggregates), γ_1 (iron carbide: $\acute{\varepsilon}$-$Fe_{2.0.2}C$), γ_2 (iron carbide-χ-$Fe_{2.5}C$), δ_1 (semi ordered sheets) and δ_2 (moderately ordered sheets) based on the peak temperatures from previous literature [40, 44, 45]. The thermal stability of the carbide is in the order $\acute{\varepsilon} < \chi < \theta$ (θ is the graphitic carbon not observed during pretreatment), corresponding to the order of the strength of the Fe–C bond [37].

Figure 6 shows that the peak temperatures for the more intense peaks are higher for Fe/Cu/K/Al and Fe/Cu/K/Zn catalysts (500–700 °C) as compared to Fe/Cu/K/Si. It is evident from the carbon content that carburization increases in the order of Fe/Cu/K/Zn > Fe/Cu/K/Al > Fe/Cu/K/Si. Based on the area under the curves and temperature assignment of the peaks, we find that α-carbon (the most reactive carbon form; C_α) increased in the order of Fe/Cu/K/Zn > Fe/Cu/K/Al > Fe/Cu/K/Si. Higher content of C_α can result in increased initial higher activity of the catalyst [44]. C_α can also condense to the C_δ form of carbon during pretreatment or a reaction run where C_δ form is graphitic carbon films having very low reactivity [44]. During pretreatment or reaction, some part of the atomic surface carbon is converted to a polymeric form of amorphous, condensed β carbon (C_β) of moderate reactivity [44]. The amount of C_β carbon increases in the order Fe/Cu/K/Al > Fe/Cu/K/Zn > Fe/Cu/K/Si. The total amount of carbides ($\gamma_1 + \gamma_2$) is highest for Fe/Cu/K/Zn and is lowest for Fe/Cu/K/Si. For Fe/Cu/K/Zn catalyst, the increase in the amount of γ_2 carbides is significant, suggesting that the catalyst has higher amount of more thermally stable carbides. The total amount of carbides ($\gamma_1 + \gamma_2$) obtained from TPH increases in the same order as the increased

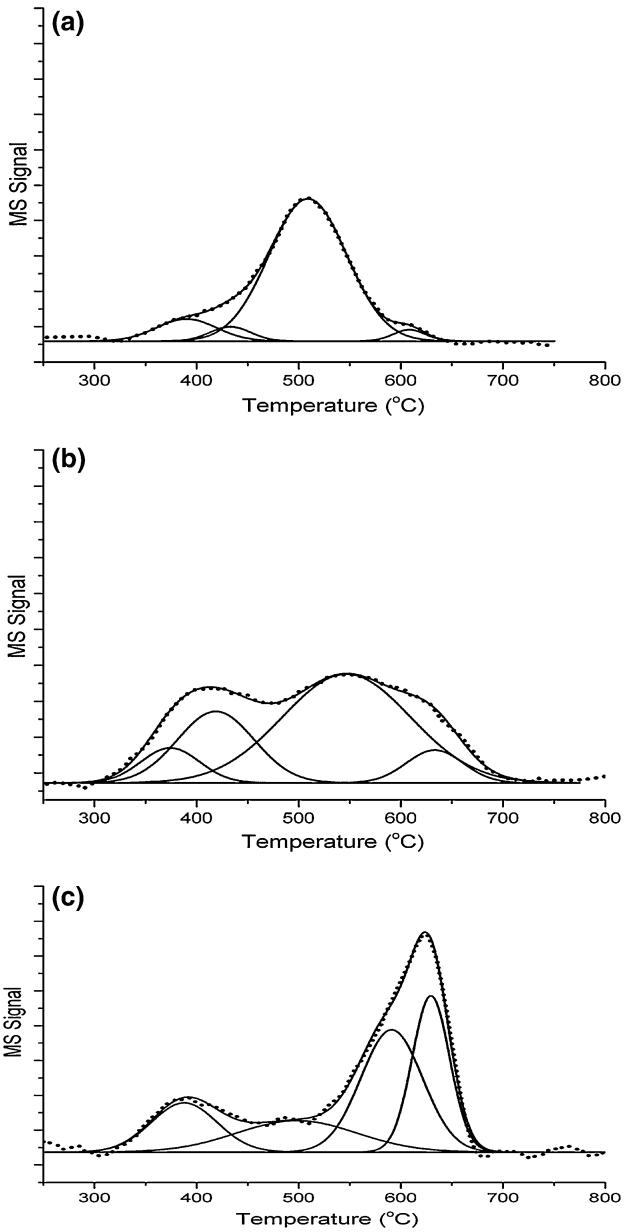

Fig. 6 TPH curves of the catalysts after activation in 5 % CO/He (**a**) Fe/Cu/K/Si, (**b**) Fe/Cu/K/Al (**c**) Fe/Cu/K/Zn

Table 4 Temperature programmed hydrogenation results after pretreatment of catalysts in 5 % CO/He

Catalyst name	Type of carbon species[a]	Peak temperature (°C)	Carbon content (μgm/gmcat)	Percentage (%)
Fe/Cu/K/Si	α	385	2.9	11.8
	β	429	1.3	5.1
	γ_1	508	19.6	79.5
	γ_2	608	0.9	3.6
Fe/Cu/K/Al	α	374	4.4	8.7
	β	420	11.8	23.2
	γ_1	547	29.9	59.0
	γ_2	633	4.6	9.1
Fe/Cu/K/Zn	α	387	7.2	13.6
	β	498	8.1	15.3
	γ_1	591	18.0	34.0
	γ_2	629	19.7	37.1

[a] See Ref. [44]

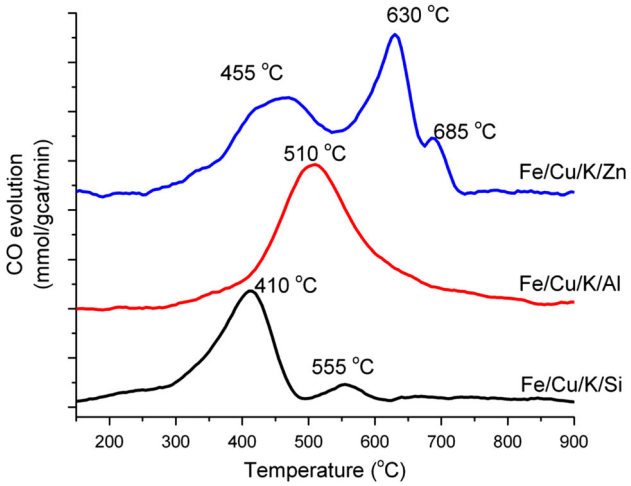

Fig. 7 Temperature programmed desorption of CO from the carbided catalysts

reduction and carburization of the catalysts in CO, specifically Fe/Cu/K/Zn > Fe/Cu/K/Al > Fe/Cu/K/Si [37]. The content of the more thermally stable carbides also increases in the same order.

4.8 CO Temperature Programmed Desorption

CO TPD is used to analyze the effect of Si, Al and Zn promotion on CO adsorption behavior of the catalysts. CO TPD curves are presented in Fig. 7. For Fe/Cu/K/Si, the desorption temperatures are in the temperature range 300–600 °C, with peaks at 410 and 555 °C, while for the Fe/Cu/K/Al the desorption occurs from a broad peak in the temperature range of 350–700 °C with a peak temperature of 510 °C. For the Fe/Cu/K/Zn catalyst, desorption temperature are in the range of 350–750 °C with two different peaks at 455 and 630 °C and a small shoulder at 685 °C.

Table 5 Amount of CO desorbed from catalyst surfaces during CO Temperature Programmed Desorption

Catalyst name	Amount of CO desorbed (μmol/gcat)
Fe/Cu/K/Si	235
Fe/Cu/K/Al	349
Fe/Cu/K/Zn	529

Desorption temperatures are lowest for Fe/Cu/K/Si with peaks at 410 and 555 °C. For Fe/Cu/K/Al catalyst, desorption peak shifts to a higher temperature and the desorption spectra shows a multipeak overlapped curve with a peak temperature at 510 °C. Studies on the desorption of CO from clean Fe (100) surfaces [46–49] suggest that CO desorbs from a Fe (100) surface to produce four CO TPD peaks, three of which are attributed to desorption of molecular CO at temperature of −23, 67, and 157 °C, while the fourth peak at ∼527 °C is ascribed to desorption of CO adsorbed dissociatively and recombined to desorb at this temperature [50]. The desorption temperatures of CO in this study from carburized surfaces on all three catalysts studied here are higher than those of molecular CO on Fe (100) surface and closer to the desorption temperature of dissociative CO ∼527 °C [50, 51] in case of Fe/Cu/K/Al. Also based on previous studies, the required desorption temperature of CO from Fe_5C_2 surfaces is about 500 °C [50, 52].The higher desorption temperature of 630 °C and small shoulder at 685 °C for Fe/Cu/K/Zn catalyst could result from the strongly bound CO on iron carbide surfaces [50]. From the area under the curves in Table 5 the amount of CO adsorbed is highest on Fe/Cu/K/Zn and least for Fe/Cu/K/Si. CO TPD results, along with TPH and CO–TPR results, show that the higher the extent of reduction and carburization, the higher the amount of CO adsorbed as measured CO TPD.

4.9 Fischer–Tropsch Synthesis

The effect of Si, Al and Zn promotion on Fe/Cu/K based catalysts for total carbon conversion ($CO + CO_2$) as a function of reaction time is shown in Fig. 8. For calculating conversion, the possibility of products being formed from both CO and CO_2 must be considered. CH_4 present in the reactant gas mixture is assumed to be inert. CO_2 can either undergo reverse water gas shift to CO and subsequently undergo FTS, or directly hydrogenate to hydrocarbons or react with H_2 to form methanol [14, 53, 54]. Therefore

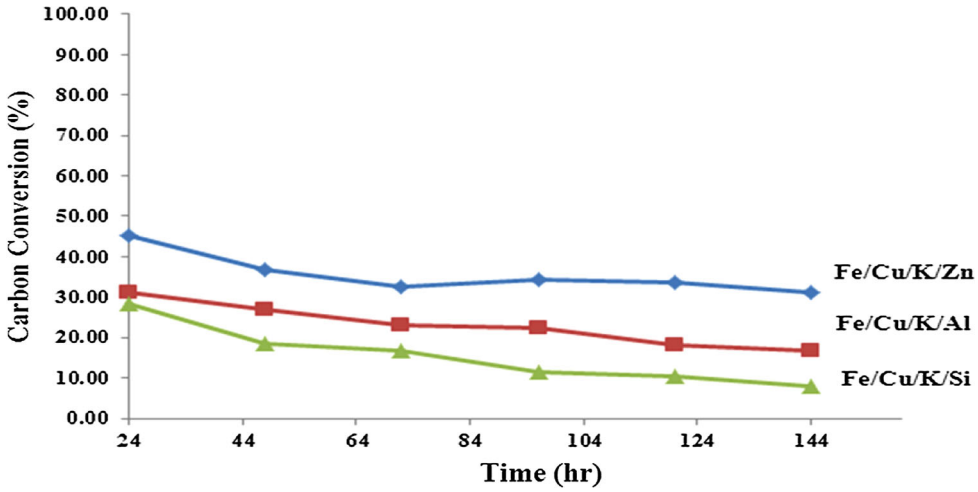

Fig. 8 Carbon conversion on Fe/Cu/K/Si, Fe/Cu/K/Al, Fe/Cu/K/Zn catalysts with time on stream (GHSV = 1,800 scc $gcat^{-1}$ h^{-1}, P = 2.8 MPa, T = 300 °C)

overall carbon conversion for the three catalysts is calculated using the equation:

$$\text{Carbon conversion} = \frac{\text{moles}(CO + CO_2)_{in} - \text{moles}(CO + CO_2)_{out}}{\text{moles } (CO + CO_2)_{in}}$$

Figure 8 shows that the carbon conversion is highest for Fe/Cu/K/Zn, while it is lowest for Fe/Cu/K/Si. Based on TPH of the carbided catalysts, iron carbide formation follows the sequence Fe/Cu/K/Zn > Fe/Cu/K/Al > Fe/Cu/K/Si. Figure 8 shows that activity of the catalysts, as measured by CO + CO_2 conversion, corresponds directly with the amount of carbides (Table 4). This clear correlation between the extent of carburization and catalytic activity is consistent with previous studies [20, 34, 51, 55].

Table 6 shows that methane selectivity decreases in the order Fe/Cu/K/Zn < Fe/Cu/K/Al < Fe/Cu/K/Si. The selectivity results in Table 6 also show that selectivity towards higher hydrocarbons (C_{19}+) is highest for Fe/Cu/K/Zn while selectivity towards methane and C_2–C_4 is suppressed. For Fe/Cu/K/Si selectivity towards methane and C_2–C_4 is high, while selectivity towards heavier hydrocarbons is suppressed. Literature shows that enhanced CO adsorption leads to higher surface coverage of carbon species thus facilitating chain growth and enhanced selectivity to heavier hydrocarbons [56]. Based on CO TPD results, we know that CO adsorption increases in the order Fe/Cu/K/Zn > Fe/Cu/K/Al > Fe/Cu/K/Si. The extent of CO adsorption could explain the high selectivity of Fe/Cu/K/Zn and Fe/Cu/K/Al towards higher hydrocarbons and the low selectivity of Fe/Cu/K/Si to C_5+ hydrocarbons. Also, the olefin/paraffin ratio is greater with the promotion by Al and Zn, suggesting slightly less hydrogenation activity on these two catalysts. Table 6 also shows that the ASF growth probability α increases in the order Zn > Al > Si. Collectively these results indicate that chain propagation and selectivity to heavier hydrocarbons is increased with Al and Zn promotion in comparison to promotion of Fe/Cu/K with Si.

Table 6 Carbon Conversion, product selectivity and olefin/paraffin ratio of catalysts, Reaction condition: 300 °C, 2.8 MPa, GHSV = 1,800 scc $gcat^{-1}$ h^{-1}

	Fe/Cu/K/Si	Fe/Cu/K/Al	Fe/Cu/K/Zn
CO + CO_2 Conversion (%)	12.98	25.19	33.69
HC distribution (C %)[a]			
CH_4	19.5	10.2	8.5
C_2–C_4	32.3	28.0	26.3
C_5–C_{11}	15.5	20.4	18.5
C_{12}–C_{18}	4.4	11.7	13.9
C_{19}+	1.51	1.84	4.56
Oxygenates	2.0	1.03	0.84
Olefins/n-Paraffins			
$C_5^=$–$C_{11}^=$/n-C_5–C_{11}	1.76	1.92	2.18
$C_{12}^=$–$C_{18}^=$/n-C_{12}–C_{18}	0.79	0.84	0.96
ASF (α)[b]	0.75	0.82	0.87

These compositions are based on a cumulative sample taken after 144 h on-stream

Reaction condition: 300 °C, 2.8 MPa, GHSV = 1,800 scc $gcat^{-1}h^{-1}$

Analysis carried out by U.Kentucky Center for Applied Energy Research

[a] Hydrocarbon selectivity is CO_2 independent

[b] Calculated using C_7–C_{15} products

Co-precipitated Fe/Cu/K/Si catalysts have been often employed for commercial FTS. However for CO_2 rich feed, previous studies have suggested [8, 23, 57], that a catalyst resistant to oxidation in CO_2 rich environment is required., The characterization results in the work reported here show that Si suppresses reduction in CO, limits carbide formation, and suppresses CO adsorption. These results are consistent with low activity of the catalyst along with high selectivity to methane and low selectivity to heavier hydrocarbons. Promotion with Zn and Al, however,

enhance reduction in CO, carbide formation and CO adsorption as compared to Fe/Cu/K/Si, resulting in high activity and selectivity to heavier hydrocarbons for the Zn or Al promoted Fe/Cu/K catalysts.

According to literature, the correlation between activity for a CO_2 rich syngas on structural promoters is dependent on the different interaction between Fe and a structural promoter [23]. Yan et al. [57] in a study on CO_2 hydrogenation reported that silica addition to Fe/Cu/K reduces the Fe and K dispersion on Si, while Al promotion enhances carburization. Jun et al. [23] also compared Si and Al structural promoters on iron based catalysts for $CO+CO_2$ hydrogenation and found that alumina as a structural promoter gave higher hydrocarbon activity than silica and had higher selectivity towards higher hydrocarbons. Jun et al. also suggested that Al_2O_3 catalyst is more easily carburized than Si catalyst, thus making the catalyst more resistant to oxidation in CO_2 rich environment. These results are consistent with our study. Based on the results in this study, it can be concluded that Fe/Cu/K/Zn is also carburized to a greater extent making it resistant to oxidation in the presence of CO_2 in the feed gas leading to high activity and selectivity to higher hydrocarbons.

5 Conclusions

Promotion of Fe/Cu/K catalyst with Si, Al or Zn greatly affects the textural properties of the catalyst, reduction of the catalyst in H_2 and CO, CO adsorption, and carburization behavior as well the activity and selectivity in FTS. The co-precipitation method used to prepare the catalysts resulted in XRD amorphous material. The catalyst promoted with Si has the highest BET surface area while incorporation of Al and Zn reduces the surface area. Reduction in CO is increased for Fe/Cu/K/Zn and Fe/Cu/K/Al as compared to Fe/Cu/K/Si. The high extent of reduction and carburization in CO for Fe/Cu/K/Zn catalyst could possibly be the reason for high catalytic activity of the catalyst in presence of CO_2 rich feed. Fe/Cu/K/Zn also shows the lowest methane selectivity and greatest selectivity to higher hydrocarbons, which appears to be due to high surface coverage of carbon species as measured by CO TPD. Fe/Cu/K/Si catalyst however had low extent of carburization and less CO adsorption resulting in reduced catalytic activity, high selectivity to methane and low selectivity to heavier hydrocarbons. These results suggest that FTS of biomass derived syngas rich in CO_2 requires a catalyst which is carburized to a higher extent, leading to higher resistance to oxidation in CO_2 rich environment.

Acknowledgments This material is based upon work funded by the U.S. Department of Agriculture, under Award Number 11-DG-11221636-187. We thank Dr. Kerry Dooley at Louisiana State University for providing the adsorbents for gas clean up, Dr. Gary Jacobs at University of Kentucky for liquid sample analysis, Ms. Wanda LeBlanc at Louisiana State University for helping in getting the XRD data and Mr. Tom Beasley at Florida International University for the SEM experiments.

References

1. Demirbas A (2007) Prog Energy Combust Sci 33(1):1–18
2. Ozcimen D, Karaosmanoglu F (2004) Renewable Energy 29:779–787
3. Jefferson M (2006) Renewable Energy 31:571–582
4. Hamelinck CN, Faaij A, den Uil H, Boerrigter H (2004) Energy 29(11):1743–1771
5. Dasgupta D, Wiltowski T (2011) Fuel 90(1):174–181
6. Davis BH (2001) Fuel Process Technol 71:157–166
7. Schulz H, Schaub G, Claeys M, Riedel T (1999) Appl Catal A 186:215–227
8. Riedel T, Claeys M, Schulz H, Schaub G, Nam S, Jun K, Choi M, Kishan G, Lee K (1999) Appl Catal A 186(1–2):201–213
9. Jun KW, Roh HS, Kim KS, Ryu JS, Lee KW (2004) Appl Catal A 259(2):221–226
10. Ubilla P, Garcia R, Fierro JLG, Escalona N (2010) J Chil Chem Soc 55(1):35–38
11. Krishnamoorthy S, Li A, Iglesia E (2002) Catal Lett 80(1–2):77–86
12. Tijmensen MJA, Faaij APC, Hamelinck CN, van Hardeveld MRM (2002) Biomass Bioenergy 23(2):129–152
13. Boerrigter H, den Uil H, Calis HP (2003) Green diesel from biomass via Fischer–Tropsch synthesis. CPL Press, Newbury, pp 371–383
14. Prasad PSS, Bae JW, Jun K-W, Lee K-W (2008) Catal Surv Asia 12:170–183
15. Yates IC, Satterfield CN (1989) Ind Eng Chem Res 28(1):9–12
16. Chun D, Lee H-T, Yang J-I, Kim H-J, Yang J, Park J, Kim B-K, Jung H (2012) Catal Lett 142(4):452–459
17. Bukur DB, Lang XS, Rossin JA, Zimmerman W, Rosynek M, Yeh EB, Li CP (1989) Ind Eng Chem Res 28:1130–1140
18. Lohitharn N, Goodwin JG, Lotero E (2008) J Catal 255:104–113
19. Elder T, Groom LH (2011) Biomass Bioenergy 35(8):3522–3528
20. Vasireddy S, Campos A, Miamee E, Adeyiga A, Armstrong R, Allison JD, Spivey JJ (2010) Appl Catal A 372(2):184–190
21. Lohitharn N, Goodwin JG, Lotero E (2008) J Catal 257:142–151
22. Tavakoli A, Sohrabi M, Kargari A (2008) Chem Eng J 136(2–3):358–363
23. Jun K-W, Roh H-S, Kim K-S, Ryu J-S, Lee K-W (2004) Appl Catal. A 259:221–226
24. Dry ME (1981) Catalysis-Science and Technology. Springer-Verlag, New York
25. Sudsakorn K, Goodwin JG, Jothimurugesan K, Adeyiga AA (2001) Ind Eng Chem Res 40:4778–4784
26. Bukur D, Koranne M, Lang X, Roa KRPM, Huffman GP (1995) Appl Catal A 126:85–113
27. Raje AP, O'Brien RJ, Davis BH (1998) J Catal 180:36–43
28. Bukur DB, Lang X, Mukesh D, Zimmerman W, Rosynek M, Li C (1990) Ind Eng Chem Res 29:1588–1599
29. Deckwer W, Lehmann HJ, Ralek M, Schmidt B (1981) Chem Ing Tech 53(10):818–819
30. GPvd Laan, Beenackers AACM (1999) Catal Rev 41(3–4):255–318
31. Herranz T, Rojas S, Perez-Alonso FJ, Ojeda M, Terreros P, Fierro JLG (2006) Appl Catal A 311:66–75

32. Nakhaei Pour A, Shahri SMK, Bozorgzadeh HR, Zamani Y, Tavasoli A, Marvast MA (2008) Appl Catal A 348(2):201–208
33. Wan H-J, Wu B-S, An X, Li T-Z, Tao Z-C, Xiang H-W, Li U-W (2007) J Nat Gas Chem 16:130–138
34. Li S, Li A, Krishnamoorthy S, Iglesia E (2001) Catal Lett 77(4):197–205
35. Luo M, Davis BH (2013) Appl Catal A 246:171–181
36. Li S, Krishnamoorthy S, Li A, Meitzner GD, Iglesia E (2002) J Catal 206:202–217
37. Nakhaei Pour A, Housaindokht MR, Zarkesh J, Tayyari SF (2010) J Ind Eng Chem 16(6):1025–1032
38. Farrauto RJ, Bartholomew CH (1997) Fundamentals and Practice. Chapman and Hall, London
39. Eliason SA, Bartholomew CH (1999) Appl Catal A 186(1–2):229–243
40. Eliason SA, Bartholomew CH (1997) In: Studies in Surface Science and Catalysis Catalyst vol. 111 Deactivation. Elsevier, Amsterdam
41. Bartholomew CH (1991). In: Guczi L (ed) Studies in Surface Science and Catalysis, vol 64. Elsevier, Amsterdam pp 158–224
42. Amelse JA, Butt JB, Schwartz LH (1978) J Phys Chem 82:558
43. Herranz T, Rojas S, Perez-Alonso FJ, Ojeda M, Terreros P, Fierro JLG (2006) J Catal 243:199–211
44. Xu J, Bartholomew CH (2005) J Phys Chem B 109:2392–2403
45. Bartholomew CH (1982) Catal Rev 24(1):67
46. Moon DW, Dwyer DJ, Bernasek SL (1985) Surf Sci 163:215–229
47. Amenomiya Y, Pleizier G (1973) J Catal 28:442–454
48. Cameron SD, Dwyer DJ (1988) Surf Sci 198:315–330
49. Benziger J, Madix RJ (1980) Surf Sci 94:119–153
50. Zhang C, Zhao G, Liu K, Yang Y, Xiang H, Li Y (2010) J Mol Catal A 328:35–43
51. Zhang H, Ma H, Zhang H, Ying W, Fang D (2012) Catal Lett 142:131–137
52. Cao D-B, Zhang F-Q, Li Y-W, Jiao H-J (2004) J Phys Chem B 108(26):9094–9104
53. Lee J, Chern W, Lee M, Dong T (1992) Can J Chem Eng 70:511–515
54. Fujimoto K, Shikada T (1987) Appl Catal 31:13–23
55. Zhang C-H, Yang Y, Teng B-T, Li T-Z, Zheng H-Y, Xiang H-W, Li Y-W (2006) J Catal 237(2):405–415
56. Wan H, Wu B, Zhang C, Xiang H, Li Y (2008) J Mol Catal A 283:33–42
57. Yan S, Jun K, Hong J, Choi M, KW L (2000) Appl Catal A 194–195:63–70